EEET ECOLOGICAL ENGINEERING & ENVIRONMENTAL TECHNOLOGY

Ecological Engineering & Environmental Technology, 2026, 27(3), 368–383
https://doi.org/10.12912/27197050/218247
ISSN 2719–7050, License CC-BY 4.0

Received: 2026.01.28
Accepted: 2026.02.25
Published: 2026.03.01

Tidal-driven variability of dissolved heavy metals and pollution index assessment in a tropical coastal system (Makassar, Indonesia)

Ratna Musa[1], Muh Ilham Anggamulia[2*], Gusnawati[3], Sattar Yunus[2], Jabbar Thaariq[2], Wan Syafrizal[2]

[1] Department of Civil Engineering, Universitas Muslim Indonesia, Makassar, Indonesia
[2] Department of Environmental Engineering, Universitas Muslim Indonesia, Makassar, Indonesia
[3] Department of Chemical Engineering, Universitas Muslim Indonesia, Makassar, Indonesia
* Corresponding author's e-mail: ilhamangga.mulia@umi.ac.id

ABSTRACT

Urbanized tropical coastal waters are increasingly exposed to heavy metal contamination due to rapid urbanization, industrial development, and domestic wastewater discharges, yet the role of tidal dynamics in regulating metal accumulation remains insufficiently understood. This study investigates the concentration patterns, tidal variability, and pollution status of dissolved heavy metals in the coastal waters of Makassar, Indonesia. Seawater samples were collected from ten representative riverine-coastal sites under contrasting high- and low-tide conditions and analyzed for Ba, Fe, Mn, Co, Ni, Cr, Zn, Pb, and Cd using Inductively coupled plasma optical emission spectrometry (ICP-OES). Pollution levels were assessed using the heavy metal pollution index (HPI), while metal associations and potential source characteristics were evaluated through correlation analysis and principal component analysis (PCA). The results demonstrate a clear tidal dependency, with systematically higher metal concentrations and HPI values observed during low-tide conditions, reflecting reduced hydrodynamic dilution and enhanced sediment resuspension. Multivariate analyses indicate that overall variability is primarily governed by background geochemical processes, whereas Pb and Cd are more strongly influenced by localized anthropogenic inputs. These findings highlight that tidal phase not only controls metal concentrations but also modulates source expression and cumulative pollution intensity. Incorporating tidal variability into coastal water quality assessment is therefore essential for improving contamination detection and supporting effective monitoring and management strategies in rapidly urbanizing tropical coastal regions.

Keywords: tidal dynamics, heavy metal pollution, coastal water quality, ICP-OES analysis.

INTRODUCTION

Despite increasing awareness of coastal pollution, many studies on heavy metals continue to underrepresent the regulatory influence of tidal dynamics, which play a critical role in governing dilution processes, sediment resuspension, and contaminant transport in coastal (Giménez et al., 2024; Wu et al., 2022). Heavy metal contamination has become one of the most persistent and ecologically significant threats in coastal systems worldwide. Rapid urbanization, industrial expansion, maritime activities, and untreated domestic discharges have intensified metal inputs into nearshore environments, particularly in developing coastal regions (Dehm et al., 2025; Jin et al., 2025; Mu et al., 2023). Trace metals such as lead (Pb), cadmium (Cd), chromium (Cr), nickel (Ni), and zinc (Zn) are of particular concern due to their environmental persistence, non-degradable nature, and tendency to accumulate in sediments and aquatic organisms, with well-documented ecotoxicological implications and potential human health risks through trophic transfer (Fehrenbach et al., 2025; Muis et al., 2024). Unlike many organic contaminants, heavy metals remain

chemically stable and environmentally active over prolonged periods, sustaining chronic ecological risk in rapidly developing coastal zones (Ao et al., 2025; Lo et al., 2023)

From a mechanistic perspective, coastal metal distribution is strongly influenced by tidal hydrodynamics, which govern dilution capacity, mixing intensity, estuarine circulation, and sediment re-suspension processes. These dynamic interactions regulate the exchange between dissolved and particulate phases and determine spatial redistribution patterns across river–coastal interfaces (Muis et al., 2024; Thelen et al., 2024). However, most empirical investigations rely on static or single-phase sampling approaches that inadequately capture tidal-driven variability, thereby limiting interpretation of short-term contamination dynamics. Moreover, while tidal–metal interactions have been extensively examined in temperate estuarine systems, comparable high-resolution studies in tropical urban coastal environments remain limited, despite distinct rainfall regimes, catchment characteristics, and monsoonal hydrodynamics that may alter contaminant (Jones et al., 2025; Tansel, 2024). This imbalance in geographic and climatic representation constrains the generalization of existing knowledge to tropical systems.

The Makassar coastal zone in South Sulawesi, Indonesia, exemplifies a rapidly urbanizing tropical coastal environment subjected to combined riverine and marine influences. The Jeneberang River functions as a major transport pathway for sediments and anthropogenic contaminants, influencing physicochemical conditions and coastal circulation patterns (Asih et al., 2022; Clough et al., 2025). Nevertheless, the tidal-phase-dependent variability of dissolved heavy metals in this system has not been systematically evaluated, and its implications for pollution index interpretation remain unclear. Because pollution indices such as the Heavy Metal Pollution Index (HPI) are calculated directly from measured dissolved concentrations, neglecting tidal modulation may introduce systematic bias in pollution classification, potentially leading to overestimation or underestimation of ecological risk under dynamic coastal conditions.

Therefore, this study aims to evaluate the spatial distribution and tidal-phase variability of dissolved-phase heavy metals in the Makassar coastal system under contrasting high- and low-tide conditions and to assess contamination status using an integrated pollution index approach. We hypothesize that tidal fluctuations significantly modulate dissolved metal concentrations through dilution and resuspension-driven exchange processes, resulting in measurable differences in pollution index values between tidal phases. By explicitly focusing on the dissolved fraction and its hydrodynamic modulation, this study advances understanding of short-term tidal controls on bioavailable metal forms and contributes to a more robust, tidal-aware interpretation of pollution indices in tropical urban coastal waters.

MATERIAL AND METHODS

Study area

The coastal waters of Makassar, Indonesia, represent a dynamic tropical urban coastal system influenced by intense anthropogenic pressures and strong tidal forcing. The Tanjung Bunga coastal zone is characterized by dense urban development, tourism activities, port operations, and riverine inputs transporting domestic and industrial effluents. The interaction between river discharge and marine hydrodynamics creates complex mixing processes that influence the distribution and transformation of dissolved heavy metals.

The average water column depth at the sampling sites is approximately 4 m. However, surface water samples were collected from the tidally mixed upper layer to evaluate spatial and tidal variability of dissolved heavy metals. The locations of the sampling sites are presented in Table 1, and a map of the study area is presented in Figure 1.

Sampling design and site selection

Sampling was conducted during the pre-monsoon period to minimize seasonal hydrological variability. A stratified sampling approach was adopted to represent gradients of anthropogenic influence and hydrodynamic conditions across riverine, creek, and coastal. Ten sampling stations were selected, two creeks: the Center Point of Indonesia Creek (S-1) and Bosowa Creek (S-2), four Coastal: Bosowa Coastal (S-3), Akkarena Coastal (S-4), Angin Mammiri Coastal (S-5), Tanjung Bayang Coastal (S-6), and four segments of the Jeneberang River from upstream to estuarine zones ranging from upstream areas (S-7) to the downstream estuarine zone (S-8), (S-9), and (S-10).

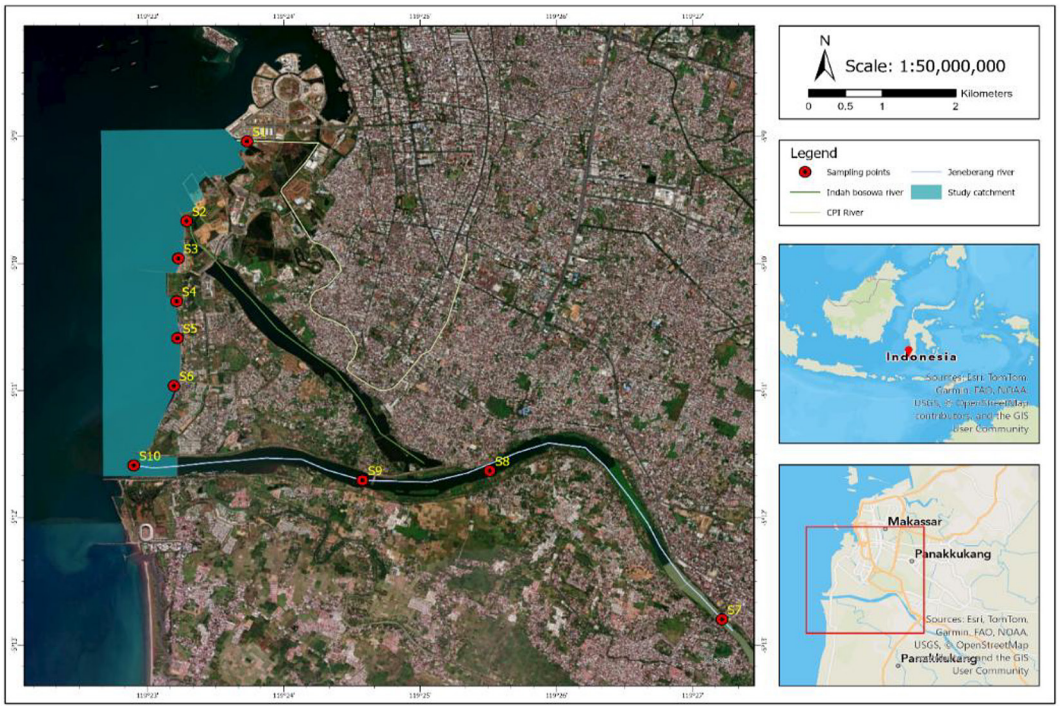

Figure 1. Overview of the study area

To examine tidal influence, sampling was performed during two contrasting tidal phases: high tide and low tide. At each station, water samples were collected under both tidal conditions using an identical standardized protocol to ensure comparability. Tidal phases were determined based on local tidal prediction data.

Preparation of sampling equipment

Prior to sampling, all equipment, including the sampler and storage bottles, were thoroughly cleaned to prevent contamination. Sampling bottles, typically 500 mL borosilicate glass or high-density polyethylene (HDPE), were acid-washed with 10% nitric acid (HNO_3) and rinsed with deionized water. The sampler was also pre-rinsed three times with ambient water at each location to eliminate any potential carry-over from previous stations.

Sampling procedure and preservation

Surface water samples were collected at approximately 30 cm below the surface using a Van Dorn horizontal water sampler (Wildco®, Yulee, Florida, USA). This depth represents the actively mixed surface layer influenced by tidal dynamics. All sampling equipment and storage bottles (500 mL HDPE or borosilicate glass) were pre-cleaned and acid-washed with 10% HNO_3, followed by rinsing with deionized water. At each station, the sampler was pre-rinsed three times with ambient water to prevent cross-contamination. Immediately after collection, samples were acidified in situ with ultrapure nitric acid (Merck Suprapur®, Darmstadt, Germany) to pH < 2 to stabilize dissolved metals. Samples were stored in dark containers at 4°C and transported to the laboratory within 24 hours.

Sample preparation (pre-analysis)

In the laboratory, samples were filtered through a 0.45 µm membrane filter (Whatman®, Maidstone, UK) to obtain the dissolved metal fraction. When required, acid digestion was performed using concentrated HNO_3 under controlled heating (85 °C for 2 hours) following APHA 3125-B and SNI 6989.16:2019 procedures.

ICP-OES measurement analysis

Metal concentrations were determined using Inductively coupled plasma optical emission spectrometry (ICP-OES; PerkinElmer Avio 500). Instrument calibration was performed using multi-element standards at five concentration levels, producing calibration curves with $R^2 > 0.995$. Quality control included reagent blanks, procedural blanks, replicate analysis, and certified reference materials. All concentrations are reported in mg/L.

Table 1. Geographic coordinates of the study area

Sample	Type of areas	Sample	Latitude ID	Longitude ID
1	Creek	S-1	-119° -23' -43.861" S	5º 9' 2.423" W
2		S-2	-119° -23' -17.254" S	5º 9' 40.021" W
3	Beach	S-3	-119° -23' -13.621" S	5º 9' 57.643" W
4		S-4	-119° -23' -12.847" S	5º 10' 17.882" W
5		S-5	-119° -23' -13.236" S	5º 10' 35.274" W
6		S-6	-119° -23' -11.688" S	5º 10' 57.745" W
7	River	S-7	-119° -27' -12.841" S	5º 12' 47.934" W
8		S-8	-119° -25' -30.659" S	5º 11' 37.835" W
9		S-9	-119° -24' -34.596" S	5º 11' 42.299" W
10		S-10	-119° -22' -53.994" S	5º 11' 35.297" W

Heavy metal pollution index (HPI)

To assess the comparative contamination potential of dissolved heavy metals across the sampling locations, the heavy metal pollution index (HPI) method was employed. The HPI index was calculated by assigning each parameter a rating or weight (W_i) ranging from 0 to 1, which represented the relative significance of multiple quality criteria when taken together. Wi could also be computed by inversely proportional to the parameter's proposed standard (S_i). The heavy metal pollution index for each metal (HPI_i) was calculated according to the following formula (Alam et al., 2023).

$$HPI = \frac{\sum_{i=1}^{n} W_i Q_i}{\sum_{i=1}^{n} W_i} \tag{1}$$

where: Q_i and W_i are the sub-index and unit weight of parameter i, respectively, and n is the number of parameters considered. The sub-index Qi is calculated by

$$Q_i = \sum_{i=1}^{n} \frac{|M_i - I_i|}{S_i - I_i} \times 100 \tag{2}$$

where: M_i represents the metal concentration measured (mg/L) obtained from ICP-OES analysis, and S_i denotes the permissible concentration limit (mg/L) as specified by the standard recommended concentration of parameters i, for Government Regulation No. 22/2021 National water quality standards. The symbol (−) stands for the numerical difference between two values, which ignores the algebraic sign.

Methods of statistical analysis

The dataset consisted of ten sampling stations analyzed under two tidal phases (high and low tide), resulting in a paired repeated measures design for nine heavy metal parameters. All measurements are presented as mean ± standard deviation (SD). The statistical procedure was performed in the following steps:

- Stage 1. Descriptive statistical analysis

Mean, standard deviation, minimum, and maximum values were calculated to summarize heavy metal concentrations across stations and tidal phases

- Stage 2. Normality assessment

Normality of paired differences (high tide – low tide) was assessed using the Shapiro–Wilk test.

- Stage 3. Homogeneity of variances

Levene's test was applied to evaluate equality of variances for spatial comparisons.

- Stage 4. Evaluation of tidal influence

Paired samples t-tests were performed for normally distributed data, whereas the Wilcoxon signed-rank test was applied when normality assumptions were not met. Bonferroni correction was used to account for multiple comparisons across nine parameters.

- Stage 5. Principal component analysis (PCA)

PCA was conducted to identify distribution patterns and potential sources of heavy metals. Components with eigenvalues > 1 were retained.

- Stage 6. Correlation analysis

Pearson correlation coefficients were calculated for normally distributed variables; otherwise, Spearman's rank correlation was applied. Statistical significance was set at $p < 0.05$.

Representative of the experimental workflow are presented in Figure 2 to enhance methodological experimental study.

RESULTS

Characteristic coastal waters

The coastal waters of the study area exhibited slightly alkaline conditions and low organic pollution during the sampling period, indicating generally acceptable baseline water quality. As shown in Table 2, surface water pH averaged 8, with moderate salinity (26 psu) and surface temperature (~30 °C). Total dissolved solids (15 mg/L) and turbidity (16 NTU) reflected moderate suspended and dissolved material loads, likely influenced by tidal mixing and sediment resuspension. Organic pollution indicators remained low, as evidenced by low biochemical oxygen demand (0.98 mg/L) and well-oxygenated conditions (6.73 mg/L DO). These physicochemical conditions provide an appropriate environmental context for interpreting tidal and spatial variability in dissolved heavy metals.

Table 2. Physicochemical parameters of the study site

No	Physicochemical parameters	Average values
1	pH	8
2	TDS (mg/l)	15
3	Turbidity (NTU)	16
4	BOD (mg/l)	0.98
5	DO (mg/l)	6.73
6	Salinity (psu)	26
7	Surface water temperature (°C)	30
8	Atmospheric temperature (°C)	32

Tidal influence on metal concentrations

Dissolved heavy metal concentrations in coastal surface waters were consistently higher during low-tide conditions than during high tide, indicating a pronounced influence of tidal dynamics on metal distribution. As shown in Tables 3 and 4, mean concentrations of most analyzed metals increased under low tide, reflecting reduced dilution by offshore seawater and enhanced contributions from land-based inputs. During high-tide conditions (Table 3; Fig. 2), the hierarchy of mean metal concentrations followed the order: Ba > Fe > Co > Mn > Ni > Zn > Cr > Pb > Cd. Barium exhibited the highest mean concentration (1.551 mg/L), followed by Fe (0.170 mg/L) and Co (0.165 mg/L), while Cd and Pb were detected at comparatively lower levels. Spatially, elevated concentrations of Ba, Fe, and Co were observed at stations S-8, S-9, and S-10, suggesting localized accumulation influenced by site-specific conditions.

In contrast, low-tide conditions (Table 4) were characterized by a marked increase in metal concentrations across most sampling stations. The mean concentration sequence remained

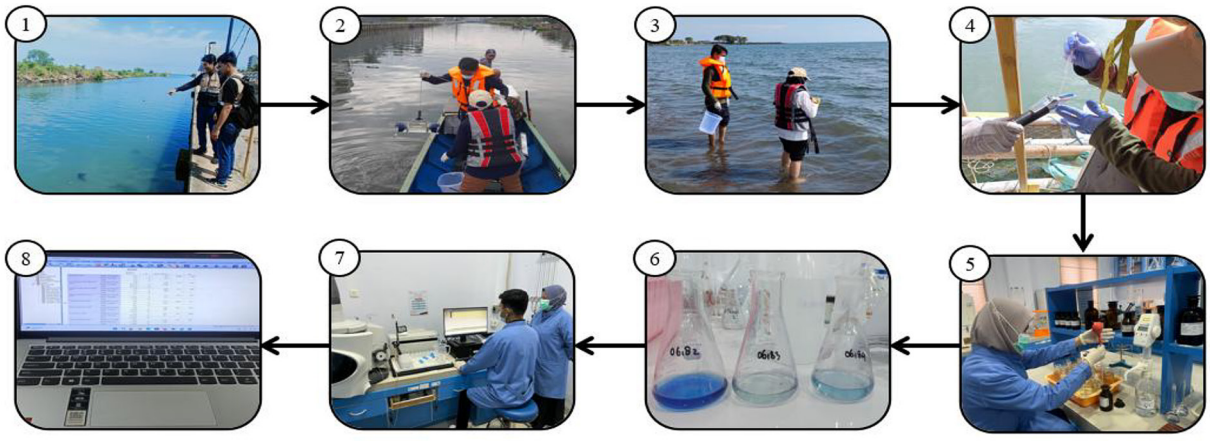

Process Description :
(1) Field survey; (2) Water sampling during high tide; (3) Water sampling during low tide; (4) In situ salinity measurement; (5) Biological parameter analysis; (6) Physicochemical parameter analysis; (7) Heavy metal analysis using ICP-OES; (8) Final data processing and reporting stage.

Figure 2. Experimental workflow diagram

broadly similar but with substantially higher values, particularly for Ba (2.767 mg/L), Fe (0.350 mg/L), and Co (0.295 mg/L). All measured concentrations during both tidal phases were well above the instrument limits of detection (LoD) determined by ICP-OES (PerkinElmer Avio 500), confirming the analytical reliability of the observed tidal-driven enrichment patterns. Notably, maximum concentrations were recorded at station S-10, where Ba, Fe, and Co reached 6.612 mg/L, 0.774 mg/L, and 0.577 mg/L, respectively. This pronounced enrichment during low tide reflects the combined influence of sediment resuspension and dominant terrestrial inflows.

The spatial distribution patterns further demonstrate that stations located near river mouths and areas with intensive anthropogenic activity exhibited consistently higher metal concentrations under both tidal regimes. However, the contrast between high- and low-tide conditions was more evident during low tide, highlighting the role of tidal flushing in regulating metal accumulation and redistribution within the coastal system. Overall, these results confirm that tidal fluctuations govern alternating dilution and enrichment processes, thereby modulating the temporal variability of dissolved heavy metals in the study area.

Heavy metal pollution index (HPI)

The calculated HPI values under high- and low-tide conditions are presented in Table 5. Overall, HPI values were consistently higher during low tide than during high tide, indicating an increase in cumulative heavy metal pollution when tidal dilution is reduced. During high tide, HPI values ranged from 29 to 117, with an average value of 72, whereas under low-tide conditions, values increased substantially, ranging from 27 to 165 with a higher mean of 99. Spatially, elevated HPI values were primarily observed at stations influenced by riverine discharge and urban industrial activities. During high tide, the highest HPI values were recorded at S-2 (117) and S-10 (111), while during low tide, S-1 (165) and S-10 (154) exhibited the most pronounced pollution levels.

In contrast, station S-7 consistently showed the lowest HPI values under both tidal regimes, suggesting relatively low cumulative metal contamination at this location. The increase in HPI values during low tide was accompanied by a higher standard deviation (45.65) compared to high tide (33.88), reflecting enhanced spatial variability in heavy metal pollution when seawater dilution is limited. These findings indicate that tidal conditions play a crucial role in modulating

Table 3. Result of average concentration of dissolved heavy metals (mg/l) during high tides

Station	Pb	Cd	Cr	Ni	Zn	Co	Mn	Fe	Ba
S-1	0.021	0.012	0.050	0.045	0.050	0.305	0.165	0.135	1.984
S-2	0.022	0.016	0.050	0.036	0.041	0.280	0.065	0.160	0.940
S-3	0.013	0.011	0.018	0.026	0.031	0.157	0.055	0.060	0.094
S-4	0.011	0.005	0.017	0.024	0.011	0.069	0.035	0.020	0.044
S-5	0.023	0.004	0.036	0.024	0.027	0.075	0.035	0.022	0.896
S-6	0.013	0.003	0.036	0.026	0.029	0.221	0.035	0.093	0.883
S-7	0.008	0.003	0.009	0.015	0.029	0.029	0.015	0.055	0.084
S-8	0.004	0.005	0.018	0.058	0.034	0.046	0.042	0.235	3.407
S-9	0.015	0.011	0.039	0.059	0.035	0.102	0.155	0.354	3.468
S-10	0.015	0.012	0.050	0.068	0.050	0.368	0.171	0.563	3.706
Min	0.004	0.003	0.009	0.015	0.011	0.029	0.015	0.020	0.044
Max	0.023	0.016	0.050	0.068	0.050	0.368	0.171	0.563	3.706
Mean	0.014	0.008	0.032	0.038	0.034	0.165	0.077	0.170	1.551
±SD	0.007	0.005	0.017	0.020	0.013	0.132	0.065	0.201	1.556
LoD	0.0065	0.0005	0.0006	0.0008	0.0003	0.0004	0.0003	0.0014	0.0000
Indonesian Standard	0.03	0.01	0.05	0.05	0.05	0.2	0.01	0.3	1
WHO Standard	0.01	0.01	0.05	0.070	No guide value	No guide value	0.04	No guide value	0.7

Table 4. Result of average concentration of dissolved heavy metals (mg/l) during low tides

Station	Pb	Cd	Cr	Ni	Zn	Co	Mn	Fe	Ba
S-1	0.039	0.018	0.087	0.057	0.066	0.442	0.246	0.365	3.456
S-2	0.037	0.017	0.056	0.048	0.050	0.361	0.140	0.370	2.564
S-3	0.017	0.013	0.037	0.036	0.041	0.245	0.082	0.165	0.943
S-4	0.015	0.007	0.036	0.035	0.032	0.172	0.066	0.182	0.969
S-5	0.022	0.006	0.046	0.039	0.035	0.157	0.093	0.259	1.975
S-6	0.026	0.007	0.046	0.037	0.034	0.145	0.089	0.276	1.861
S-7	0.004	0.003	0.009	0.002	0.029	0.003	0.052	0.206	0.064
S-8	0.008	0.006	0.018	0.058	0.034	0.368	0.171	0.354	3.468
S-9	0.016	0.013	0.052	0.069	0.046	0.482	0.381	0.553	5.757
S-10	0.021	0.014	0.080	0.080	0.064	0.577	0.439	0.774	6.612
Min	0.004	0.003	0.009	0.002	0.029	0.003	0.052	0.165	0.064
Max	0.039	0.018	0.087	0.080	0.066	0.577	0.439	0.774	6.612
Mean	0.021	0.010	0.047	0.046	0.043	0.295	0.176	0.350	2.767
±SD	0.012	0.006	0.028	0.026	0.014	0.203	0.151	0.219	2.375
LoD	0.0065	0.0005	0.0006	0.0008	0.0003	0.0004	0.0003	0.0014	0.0000
Indonesian Standard	0.03	0.01	0.05	0.05	0.05	0.2	0.01	0.3	1
WHO Standard	0.01	0.01	0.05	0.070	No guide value	No guide value	0.04	No guide value	0.7

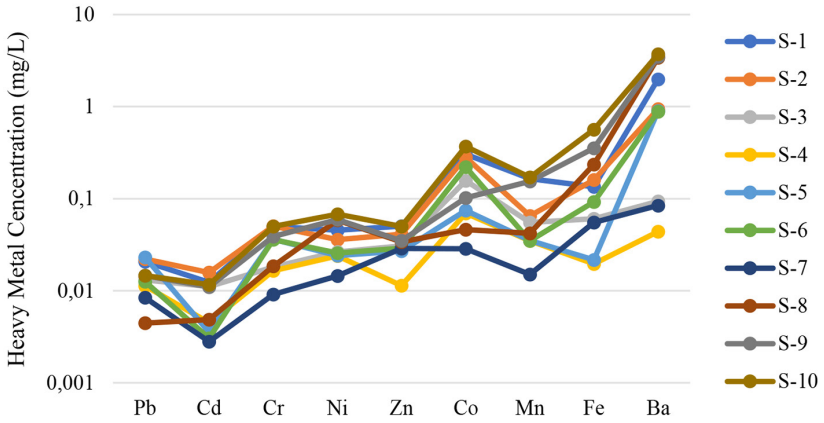

Figure 3. Heavy metal concentration of study area (high tide)

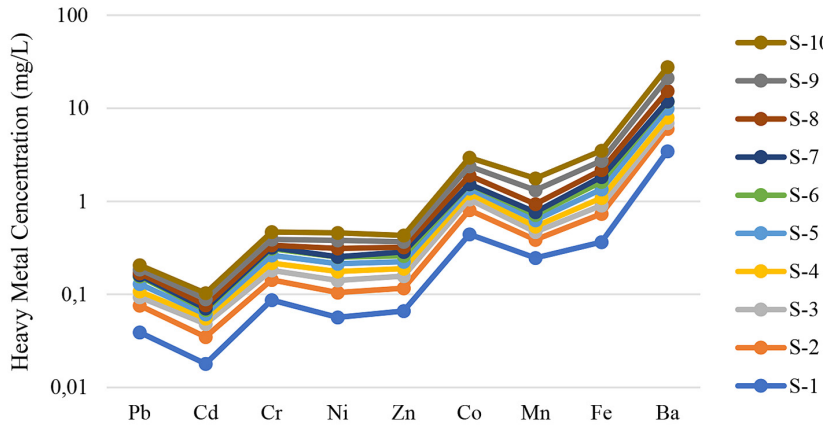

Figure 4. Heavy metal concentration of study area (low tide)

Table 5. Calculated heavy metal indices of both condition high and low tide in the studied

Location Index	Heavy metal pollution index	
	High tide (HT)	Low tide (LT)
S-1	109	165
S-2	117	142
S-3	78	101
S-4	39	66
S-5	48	71
S-6	43	73
S-7	29	27
S-8	51	69
S-9	96	128
S-10	111	154
Maximum	117	165
Minimum	29	27
Average	72	99
SD	33.88	45.65

the intensity and spatial heterogeneity of metal pollution across the study area.

Consistent with previous observations, stations located near downstream river zones and coastal industrial areas exhibited higher cumulative metal loads, highlighting the combined influence of riverine inputs and anthropogenic activities (Ardila et al., 2023). Conversely, sites characterized by reduced human disturbance or upstream riverine influence displayed comparatively lower HPI values, supporting their classification as less impacted reference locations (Lakshmanna et al., 2022; Rajendiran et al., 2025). Overall, the HPI results reinforce the strong coupling between tidal dynamics, spatial location, and cumulative heavy metal pollution in coastal surface waters.

In terms of metal-specific behavior, Fe and Pb exhibited the highest median concentrations and the widest spatial variability across sampling stations, suggesting stronger contributions from sediment resuspension processes and urban runoff inputs. In contrast, Cd and Ni displayed relatively lower concentrations but more spatially consistent distributions, indicating more uniform background levels across the study area. Meanwhile, Ba and Co showed comparatively stable concentration patterns under both tidal conditions, reflecting a predominant influence of geogenic sources such as mineral weathering and sediment water interactions (Kim et al., 2023; Uddin et al., 2024). The contrasting variability observed among metals supports the interpretation that both natural factors (e.g., mineral weathering and sediment load) and anthropogenic influences (e.g., domestic effluents and port-related

Table 6. Descriptive statistics - high tide condition

Indicator		Pb	Ba	Fe	Cd	Co	Cr	Mn	Ni	Zn
Valid N		10	10	10	10	10	10	10	10	10
Mean	Statistic	0.0145	1.5436	0.1918	0.0083	0.1626	0.0323	0.0783	0.0368	0.0337
	Std. Error	0.00195	0.47084	0.05552	0.00146	0.03928	0.00494	0.01916	0.00646	0.00365
95% Confidence Interval for Mean	Lower bound	0.0101	0.4785	0.0662	0.0050	0.0737	0.0211	0.0350	0.0222	0.0254
	Upper bound	0.0189	2.6087	0.3174	0.0116	0.2515	0.0435	0.1216	0.0514	0.0420
5% Trimmed mean		0.0146	1.5068	0.1807	0.0082	0.1601	0.0326	0.0767	0.0370	0.0341
Median		0.0140	0.9180	0.1475	0.0085	0.1295	0.0360	0.0535	0.0310	0.0325
Variance		0.000	2.217	0.031	0.000	0.015	0.000	0.004	0.000	0.000
Std. deviation		0.00615	1.48894	0.17557	0.00462	0.12422	0.01563	0.06059	0.02043	0.01154
Min		0.00	0.04	0.02	0.00	0.00	0.01	0.02	0.00	0.01
Max		0.02	3.71	0.56	0.02	0.37	0.05	0.17	0.07	0.05
Range		0.02	3.66	0.54	0.01	0.37	0.04	0.16	0.07	0.04
Interquartile Range		0.01	3.36	0.30	0.01	0.22	0.03	0.12	0.03	0.01
Skewness	Statistic	-0.102	0.548	1.107	0.242	0.435	-0.183	0.855	0.041	-0.287
	Std. error	0.687	0.687	0.687	0.687	0.687	0.687	0.687	0.687	0.687
Kurtosis	Statistic	-0.639	-1.538	0.790	-1.435	-1.245	-1.668	-1.223	-0.649	0.742
	Std. error	1.334	1.334	1.334	1.334	1.334	1.334	1.334	1.334	1.334

activities) jointly govern the overall distribution of heavy metals in coastal surface waters, with their relative contributions modulated by tidal dynamics (Xianglei et al., 2025; Zou et al., 2024).

Results of statistical analysis

Descriptive statistics

Descriptive statistics were calculated for each heavy metal parameter at all stations and tidal phases, including mean, standard deviation, minimum, and maximum values. These statistics were used to characterize the overall distribution pattern and preliminary tidal variation.

Testing the normality data

Normality tests were performed using the Kolmogorov-Smirnov and Shapiro-Wilk tests. Since the sample size for each group was n = 10 (<50), the primary interpretation was based on the Shapiro-Wilk test.

Decision-Making Criteria:
- If Sig. > 0.05 → Data are normally distributed
- If Sig. < 0.05 → Data are not normally distributed

The analysis results show that most parameters have a significance value (Sig.) > 0.05, indicating a normal distribution of the data. However, several parameters showed a Sig. value < 0.05, namely: Barium (Ba) at high tide and Manganese (Mn) at high tide, this indicates that not all variables meet the assumption of normality.

Testing the homogeneity of variance

The homogeneity test was conducted using Levene's Test to determine whether the variances between the high and low tide groups were equal (homogeneous).

Decision-making criteria:
- If Sig. > 0.05 → Homogeneous variance
- If Sig. < 0.05 → Inhomogeneous variance

The analysis results show that most parameters have a significance value (Sig.) > 0.05, indicating homogeneous data. However, several parameters showed a Sig. value < 0.05, namely: dissolved manganese (Mn). This indicates that there is a significant difference in variation between high and low tide conditions for Mn. In other words, the data distribution in both conditions is uneven.

The conclusions that can be drawn from the prerequisite test above are as follows:
- most parameters (8 of 9) have homogeneous variance,
- the Mn parameter shows non-homogeneous variance,

Table 7. Descriptive statistics – low tide condition

Indicator		Pb	Ba	Fe	Cd	Co	Cr	Mn	Ni	Zn
Valid N		10	10	10	10	10	10	10	10	10
Mean	Statistic	0.0205	2.7669	0.3504	0.0104	0.2952	0.0467	0.1759	0.0461	0.0431
	Std. Error	0.00356	0.66705	0.05949	0.00165	0.05679	0.00768	0.04323	0.00686	0.00418
95% confidence interval for mean	Lower bound	0.0125	1.2579	0.2158	0.0067	0.1667	0.0293	0.0781	0.0306	0.0336
	Upper bound	0.0285	4.2759	0.4850	0.0141	0.4237	0.0641	0.2737	0.0616	0.0526
5% trimmed mean		0.0204	2.7034	0.3372	0.0104	0.2958	0.0466	0.1682	0.0467	0.0426
Median		0.0190	2.2695	0.3150	0.0100	0.3030	0.0460	0.1165	0.0435	0.0380
Variance		0.000	4.450	0.035	0.000	0.032	0.001	0.019	0.000	0.000
Std. deviation		0.01125	2.10938	0.18814	0.00521	0.17957	0.02427	0.13670	0.02171	0.01323
Min		0.00	0.06	0.17	0.00	0.00	0.01	0.05	0.00	0.03
Max		0.04	6.61	0.77	0.02	0.58	0.09	0.44	0.08	0.07
Range		0.04	6.55	0.61	0.02	0.57	0.08	0.39	0.08	0.04
Interquartile Range		0.02	3.08	0.22	0.01	0.30	0.03	0.20	0.03	0.02
Skewness	Statistic	0.415	0.760	1.439	0.151	-0.006	0.233	1.188	-0.480	0.916
	Std. error	0.687	0.687	0.687	0.687	0.687	0.687	0.687	0.687	0.687
Kurtosis	Statistic	-0.354	-0.206	2.002	-1.525	-0.890	-0.191	0.130	1.015	-0.484
	Std. error	1.334	1.334	1.334	1.334	1.334	1.334	1.334	1.334	1.334

Table 8. Tests of normality

Variables	Condition	Kolmogorov-Smirnov[a]			Shapiro-Wilk			Result
		Statistic	df	Sig.	Statistic	df	Sig.	
Pb	High tide	0.168	10	.200*	0.949	10	0.656	Significant
	Low tide	0.147	10	.200*	0.949	10	0.660	Significant
Ba	High tide	0.257	10	0.059	0.835	10	0.038	Not Significant
	Low tide	0.170	10	.200*	0.928	10	0.427	Significant
Fe	High tide	0.172	10	.200*	0.889	10	0.167	Significant
	Low tide	0.259	10	0.057	0.858	10	0.072	Significant
Cd	High tide	0.221	10	0.184	0.889	10	0.167	Significant
	Low tide	0.243	10	0.097	0.910	10	0.284	Significant
Co	High tide	0.187	10	.200*	0.933	10	0.479	Significant
	Low tide	0.154	10	.200*	0.968	10	0.870	Significant
Cr	High tide	0.220	10	0.187	0.873	10	0.110	Significant
	Low tide	0.151	10	.200*	0.958	10	0.764	Significant
Mn	High tide	0.287	10	0.019	0.792	10	0.012	Not Significant
	Low tide	0.228	10	0.151	0.826	10	0.030	Not Significant
Ni	High tide	0.201	10	.200*	0.940	10	0.548	Significant
	Low tide	0.205	10	.200*	0.950	10	0.666	Significant
Zn	High tide	0.181	10	.200*	0.929	10	0.443	Significant
	Low tide	0.230	10	0.143	0.864	10	0.086	Significant

Note: * This is a lower bound of the true significance' (a) Lilliefors significance correction.

Table 9. Test of homogeneity of variances

Variables	Levene statistic	df1	df2	Sig.	Result
Pb	2.426	1	18	0.137	Significant
Ba	0.730	1	18	0.404	Significant
Fe	0.004	1	18	0.948	Significant
Cd	0.396	1	18	0.537	Significant
Co	2.077	1	18	0.167	Significant
Cr	0.615	1	18	0.443	Significant
Mn	4.853	1	18	0.041	Not Significant
Ni	0.002	1	18	0.962	Significant
Zn	0.564	1	18	0.462	Significant

- because there is non-normality and inhomogeneity in several variables, the use of a non-parametric test (Wilcoxon) is methodologically appropriate.

Evaluation of tidal effect

This test is used to determine whether there is a significant difference between high and low tide conditions.

Criteria:
- Sig < 0.05 → significant difference
- Sig > 0.05 → no significant difference

Based on the Wilcoxon signed rank test results, all heavy metal parameters showed a significance value less than 0.05 ($p < 0.05$). This indicates a significant difference between heavy metal concentrations at high and low tide. In general, heavy metal concentrations tended to be higher at low tide than at high tide. This phenomenon indicates that at low tide, there is an increase in metal accumulation or concentration due to reduced water volume and a weakening of the dilution process. Therefore, the hypothesis stating that there is a difference in heavy metal concentrations between high and low tide is accepted.

Table 10. Wilcoxon test

Variables	Z	Asymp. Sig. (2-tailed)	Result
Pb (LT)_Pb (HT)	-2.165[b]	0.030	Significant
Ba (LT)_Ba (HT)	-2.666[b]	0.008	Significant
Fe (LT)_Fe (HT)	-2.668[b]	0.008	Significant
Cd (LT)_Cd (HT)	-2.000[b]	0.046	Significant
Co (LT)_Co (HT)	-2.492[b]	0.013	Significant
Cr (LT)_Cr (HT)	-2.803[b]	0.005	Significant
Mn (LT)_Mn (HT)	-2.714[b]	0.007	Significant
Ni (LT)_Ni (HT)	-2.251[b]	0.024	Significant
Zn (LT)_Zn (HT)	-2.333[b]	0.020	Significant

To visually assess the distribution patterns, variability, and potential outliers of heavy metal concentrations across sampling stations and tidal phases, box plot analysis was performed for the nine investigated metals (Figure 5).

Interpretation principal component analysis

The principal component analysis (PCA) was applied to identify dominant patterns and potential controlling factors influencing the distribution of dissolved heavy metals under contrasting tidal conditions. For both high and low tide datasets, two principal components (PC) with eigenvalues greater than 1 were retained, indicating that a limited number of factors explain most of the variance in metal concentrations (Table 6). Under high tide conditions, PC1 exhibited an eigenvalue of 5.63 and accounted for 62.51% of the total variance.

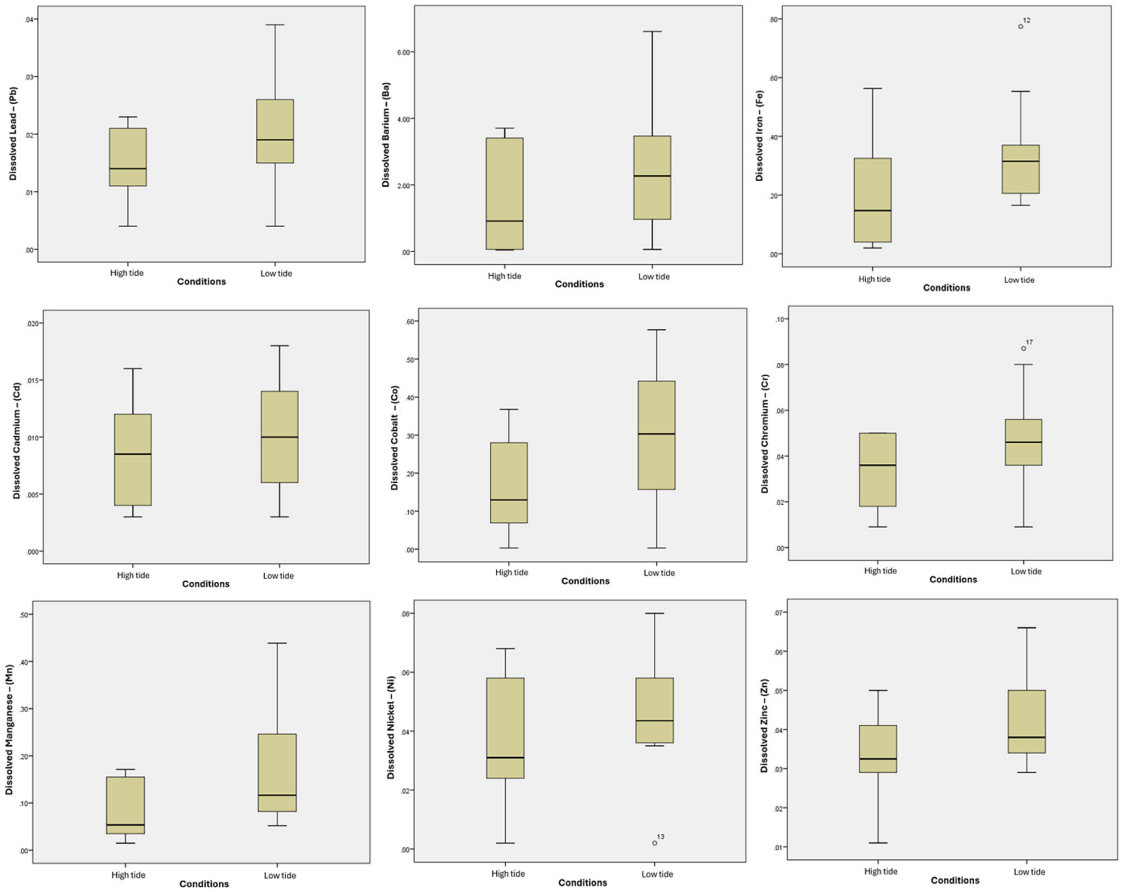

Figure 5. Box plots for the nine study samples of heavy metal

This component showed strong positive loadings for Mn, Zn, Cr, Ni, Fe, Co, Ba, and Cd, suggesting a common controlling influence affecting the majority of metals. In contrast, Pb displayed a relatively low loading on PC1 but showed the highest positive loading on PC2. PC2, with an eigenvalue of 1.99, explained an additional 22.09% of the variance, resulting in a cumulative variance of 84.59%. The separation of Pb from other metals along PC2 indicates a distinct behavior compared to the bulk metal assemblage during high tide. During low-tide conditions, PC1 became more dominant, with an eigenvalue of 6.67 explaining 74.14% of the total variance. Strong positive loadings were observed for Co, Zn, Ni, Mn, Ba, Cr, and Fe, indicating a tighter association among these metals when tidal dilution was reduced. PC2, with an eigenvalue of 1.66, accounted for 18.47% of the variance, increasing the cumulative variance to 92.60%. Similar to high tide, Pb and Cd exhibited strong positive loadings on PC2, while Mn, Fe, Ba, and Ni were negatively associated with this component.

The enhanced dominance of PC1 under low-tide conditions reflects stronger coupling among metals, likely driven by reduced seawater dilution and increased influence of sediment water interactions and terrestrial inputs. Overall, the PCA results highlight clear tidal contrasts in metal association patterns and support the presence of multiple controlling factors governing heavy metal distribution in coastal surface waters.

Correlation analysis

The Pearson correlation analysis was conducted to further examine inter-metal relationships in coastal surface waters under contrasting tidal conditions, with correlation coefficients summarized in Table 8. Overall, the correlation patterns were consistent with the PCA structure, showing stronger and more coherent associations among metals during low tide compared to high tide. During high-tide conditions, several metals, including Mn, Zn, Ni, Cr, and Fe, exhibited significant positive correlations with one another, indicating shared controlling processes under enhanced seawater dilution. In contrast, Pb showed weak or negative correlations with most metals, while Cd displayed limited associations, reflecting distinct behavior relative to the main metal group. This separation is consistent with the PCA results, where Pb and Cd were isolated along the second principal component, as indicated by the eigenvalue structure in the scree plot (Fig. 6) and their positioning in the high tide biplot (Fig. 7).

Under low-tide conditions, correlation coefficients generally increased, revealing stronger inter-metal coupling across the study area. Co, Zn, Ni, Mn, Fe, and Ba formed a tightly correlated assemblage, as reflected by both high correlation values in Table 8 and their clustered distribution along PC1 in the low-tide biplot (Fig. 7). Conversely, Pb and Cd continued to exhibit weaker or selective correlations, aligning with their separation along PC2 and confirming their distinct contribution to overall metal variability.

The enhanced strength and consistency of correlations during low tide correspond with the increased dominance of the first principal component observed in the scree plot (Fig. 6), which explains a larger proportion of total variance under reduced tidal dilution. Collectively, the correlation analysis reinforces the PCA interpretation by

Table 11. Analysis of the main components of heavy metals in coastal water samples for high and low tide conditions

Variables	High tide		Low tide	
	PC1	PC2	PC1	PC2
Pb	0.164	0.588	0.210	0.613
Cd	0.322	0.238	0.309	0.378
Cr	0.356	0.297	0.336	0.313
Ni	0.351	-0.365	0.354	-0.182
Zn	0.373	0.061	0.355	0.220
Co	0.334	0.280	0.371	-0.118
Mn	0.384	-0.040	0.351	-0.297
Fe	0.346	-0.338	0.336	-0.319
Ba	0.319	-0.421	0.350	-0.312

Table 12. The correlation matrix of heavy metals

Variables	High tide			Low tide		
	Eigenvalue	Variance	Cumulative	Eigenvalue	Variance	Cumulative
Pb	5.6256	62.51%	62.51%	6.6723	74.14%	74.14%
Cd	1.9877	22.09%	84.59%	1.6619	18.47%	92.60%
Cr	0.4825	5.36%	89.95%	0.2793	3.10%	95.70%
Ni	0.3760	4.18%	94.13%	0.2350	2.61%	98.32%
Zn	0.2285	2.54%	96.67%	0.0869	0.97%	99.28%
Co	0.1810	2.01%	98.68%	0.0406	0.45%	99.73%
Mn	0.0953	1.06%	99.74%	0.0224	0.25%	99.98%
Fe	0.0229	0.25%	99.99%	0.0014	0.02%	100.00%
Ba	0.0005	0.01%	100.00%	0.0002	0.00%	100.00%

Table 13. Correlation analysis of heavy metals during the high tide and low tide

	Pb	Cd	Cr	Ni	Zn	Co	Mn	Fe	Ba
High tide									
Pb	1								
Cd	0.497	1							
Cr	0.740	0.656	1						
Ni	-0.066	0.484	0.504	1					
Zn	0.346	0.687	0.731	0.648	1				
Co	0.493	0.690	0.824	0.414	0.764	1			
Mn	0.328	0.677	0.708	0.772	0.754	0.653	1		
Fe	-0.075	0.455	0.499	0.900	0.643	0.502	0.750	1	
Ba	-0.112	0.307	0.456	0.967	0.605	0.288	0.704	0.873	1
Low tide									
Pb	1								
Cd	0.757	1							
Cr	0.796	0.813	1						
Ni	0.341	0.609	0.680	1					
Zn	0.670	0.880	0.922	0.708	1				
Co	0.378	0.746	0.713	0.956	0.826	1			
Mn	0.172	0.539	0.648	0.869	0.744	0.900	1		
Fe	0.172	0.458	0.609	0.833	0.697	0.845	0.956	1	
Ba	0.207	0.501	0.628	0.934	0.691	0.917	0.973	0.956	1

demonstrating that tidal dynamics not only influence the magnitude of metal concentrations but also regulate the structure and strength of inter-metal relationships in coastal surface waters.

DISCUSSION

The present study demonstrates that tidal-driven variability exerts a fundamental control over both the magnitude and structure of dissolved heavy metal contamination in tropical coastal waters. In the Makassar coastal system, contrasts between high and low tide conditions reflect a dynamic coupling between hydrodynamic dilution, sediment water exchange, and land-based pollutant inputs across riverine and coastal zones. Beyond dilution effects, metal concentrations are further modulated by site-specific physicochemical conditions and anthropogenic settings, including settlement density, organic matter inputs, pH-dependent metal speciation, and adsorption-desorption processes involving suspended particulate matter. These controls

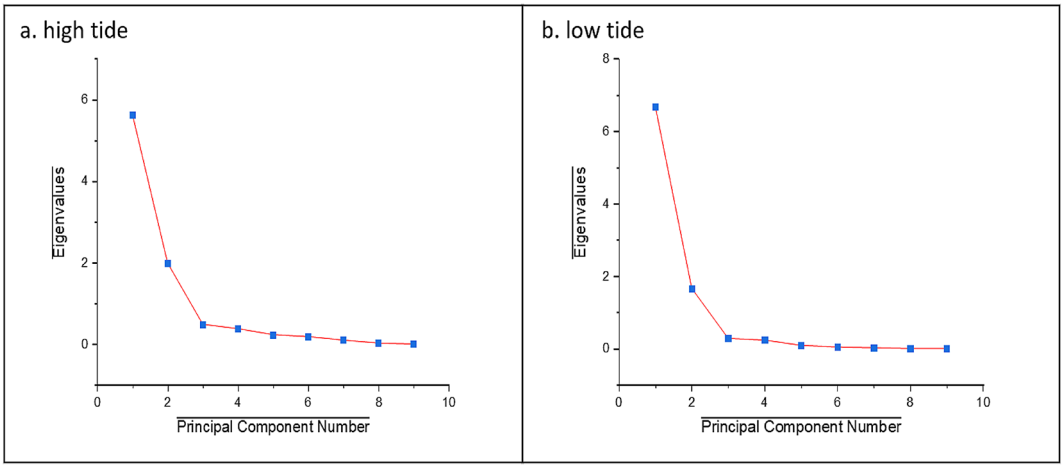

Figure 6. Scree plot of principal component eigenvalues between high tide (a) and low tide (b) conditions

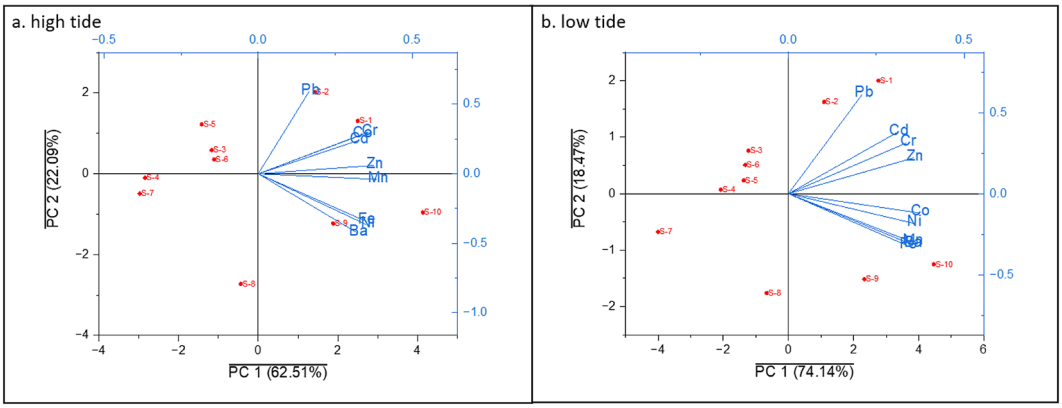

Figure 7. PCA biplot of heavy metals under high tide (a) and low tide (b) conditions

become particularly influential during low tide, when reduced water depth enhances electrical conductivity and total dissolved solids, intensifies sediment resuspension, and limits seawater mixing, thereby promoting higher metal mobility and accumulation at sites influenced by river discharge and urban runoff (Zou et al., 2024).

Multivariate analyses further clarify the governing mechanisms behind these patterns. The dominance of PC1 under both tidal phases, especially during low tide indicates that a coherent assemblage of metals (Mn, Fe, Zn, Ni, Cr, Co, and Ba) primarily reflects background geochemical controls associated with sediment resuspension, riverine material transport, and hydrodynamic mixing (Wu et al., 2022). The strengthening of inter-metal correlations and tighter clustering in PCA space under low-tide conditions, together with elevated HPI values, confirms that reduced tidal dilution amplifies existing metal accumulation processes rather than introducing new contamination sources (Khodja et al., 2025). In contrast, Pb and Cd exhibit distinct behavior, characterized by their separation along PC2 and more variable correlation patterns, particularly during low tide. Their decoupling from sediment-associated metals indicates localized anthropogenic inputs that become more pronounced when hydrodynamic dilution is constrained, especially at urban and infrastructure-dominated sites such as Centre Point of Indonesia (S-1), Akkarena (S-4), and Angin Mammiri (S-5). The spatial concordance between PC2 dominance, stronger Pb and Cd associations, and elevated HPI values at these sites supports a dual-source contamination mechanism, whereby natural background processes are modulated by tidal dynamics and overlaid by anthropogenic loading (Lucia et al., 2023).

Overall, the results demonstrate that tidal oscillation functions as a dominant regulatory mechanism controlling not only the magnitude but also the structural organization of dissolved heavy

metals in coastal waters. The consistent enrichment of all nine metals during low tide confirms that reduced marine dilution and enhanced riverine and sedimentary influence systematically intensify contamination signals across chemically distinct elements. More importantly, tidal phase amplifies spatial heterogeneity, as reflected by the increased HPI mean and variance under low tide conditions, indicating that weakened hydrodynamic flushing exposes intrinsic contamination gradients that may remain masked during high tide. Multivariate analyses further reveal structural reorganization of metal associations, with stronger covariance and greater variance explained by PC1 under low tide, suggesting convergence toward shared sources or mobilization pathways when dilution is minimized. The differentiated behavior of Pb and Cd implies additional anthropogenic inputs operating alongside geogenic and sediment-controlled processes. Collectively, these findings establish tidal forcing as a dynamic switch between dilution-dominated and concentration-dominated regimes, with direct implications for monitoring strategy and ecological risk assessment, particularly in river-influenced coastal systems where hydrodynamic timing critically shapes contaminant expression.

CONCLUSIONS

This study demonstrates that tidal phase is a dominant regulator of heavy metal dynamics in coastal waters. Concentrations of all nine metals were consistently higher during low tide, indicating reduced dilution and enhanced influence of riverine inputs and sediment–water interactions. The increase in HPI values and strengthened multivariate associations under low tide confirm that tidal oscillation not only elevates contamination levels but also restructures inter-metal relationships. High tide conditions promote hydrodynamic mixing and partial homogenization, whereas low tide amplifies spatial heterogeneity and reveals contamination hotspots. The distinct behavior of Pb and Cd further suggests mixed geogenic and anthropogenic contributions. These findings highlight the necessity of incorporating tidal phase into monitoring protocols and ecological risk assessment, as sampling without tidal standardization may underestimate cumulative metal pressure. Tidal-driven variability should therefore be recognized as a critical factor in coastal environmental management and pollution control strategies.

Acknowledgements

The authors extend their profound gratitude to the Directorate of Research and Community Service (DPPM) of the Ministry of Higher Education, Science, and Technology, Republic of Indonesia, for the financial support granted to cover the publication fees of this research article, and support from the Research and Development Institute (LP2S) Universitas Muslim Indonesia. We take this opportunity to convey our highest appreciation and sincere acknowledgement for their invaluable support

REFERENCES

1. Alam, M.J., Kamal, A.S.M.M., Ahmed, M.K., Rahman, M., Hasan, M., & Rahman, S.A.R. (2023). Nutrient and heavy metal dynamics in the coastal waters of St. Martin's island in the Bay of Bengal. *Heliyon*, *9*(10). https://doi.org/10.1016/j.heliyon.2023.e20458
2. Ao, M., Zhou, R., Meng, R., Bonaventure, L.A., Luo, B., Qian, X., Xu, X., Wang, S., & Wu, P. (2025). Chromium transformations and biological impacts in aquatic systems: From sediment-water interfaces to food web complexity. *Ecotoxicology and Environmental Safety*, *303*, 118850. https://doi.org/https://doi.org/10.1016/j.ecoenv.2025.118850
3. Ardila, P.A.R., Alonso, R.Á., Valsero, J.J.D., García, R.M., Cabrera, F.Á., Cosío, E.L., & Laforet, S.D. (2023). Assessment of heavy metal pollution in marine sediments from southwest of Mallorca island, Spain. *Environmental Science and Pollution Research*, *30*(7), 16852–16866. https://doi.org/10.1007/s11356-022-25014-0
4. Asih, A.S., Zamroni, A., Alwi, W., Sagala, S.T., & Putra, A.S. (2022). Assessment of heavy metal concentrations in seawater in the coastal areas around Daerah Istimewa Yogyakarta Province, Indonesia. *Iraqi Geological Journal*, *55*(1), 14–22. https://doi.org/10.46717/igj.55.1B.2Ms-2022-02-18
5. Clough, T.W., Silvester, R., Kevill, J., Farkas, K., Malham, S.K., Cross, G., Robins, P., & Jones, D.L. (2025). Predicting norovirus contamination and antimicrobial resistance in coastal waters from community and hospital-derived sources. *Water Research*, 124555. https://doi.org/https://doi.org/10.1016/j.watres.2025.124555
6. Dehm, J., Le Gendre, R., Lal, M., Menkes, C., & Singh, A. (2025). Water quality within the greater Suva urban marine environment through spatial analysis of nutrients and water properties. *Marine Pollution Bulletin*, *213*, 117601. https://doi.org/https://doi.org/10.1016/j.marpolbul.2025.117601

7. Fehrenbach, G.W., Murphy, E., Tanoeiro, J.R., Pogue, R., & Major, I. (2025). Monitoring water contamination through shellfish: A systematic review of biomarkers, species selection, and host response. *Ecotoxicology and Environmental Safety*, *295*, 118120. https://doi.org/https://doi.org/10.1016/j.ecoenv.2025.118120
8. Giménez, J.G., Granero, A., Senent-Aparicio, J., Gómez-Jakobsen, F., Mercado, J.M., Blanco-Gómez, P., Ruiz, J.M., & Cecilia, J.M. (2024). Assessment of oceanographic services for the monitoring of highly anthropised coastal lagoons: The Mar Menor case study. *Ecological Informatics*, *81*, 102554. https://doi.org/https://doi.org/10.1016/j.ecoinf.2024.102554
9. Jin, L., Ding, L., Zhang, Y., Li, T., & Liu, Q. (2025). Profiling heavy metals distribution in surface sediments from the perspective of coastal industrial structure and their impacts on bacterial communities. *Ecotoxicology and Environmental Safety*, *294*, 118098. https://doi.org/https://doi.org/10.1016/j.ecoenv.2025.118098
10. Jones, M.L., Clare Leonard, A.F., Bethel, A., Lamb, E., Gaze, W.H., Taylor, T., Singer, A.C., Ukoumunne, O.C., & Garside, R. (2025). Recreational exposure to polluted open water and infection: A systematic review and meta-analysis protocol. *Environment International*, *200*, 109371. https://doi.org/https://doi.org/10.1016/j.envint.2025.109371
11. Khodja, H.D., Aichour, A., Metaiche, M., & Ferhati, A. (2025). Hydrochemical Assessment of Albian Waters of Southern Algeria Using Water Quality Indices. *Polish Journal of Environmental Studies*, *34*(5), 5599–5605. https://doi.org/10.15244/pjoes/191968
12. Kim, H.-C., Son, S., Ok Jo, C., Hoon Kim, Y., Park, M., Park, Y.-G., & Ryu, J. (2023). Spatio-temporal structures of satellite-derived water quality indicators along the Korean South Coast. *Environment International*, *178*, 108083. https://doi.org/https://doi.org/10.1016/j.envint.2023.108083
13. Lakshmanna, B., Jayaraju, N., Sreenivasulu, G., Lakshmi Prasad, T., Nagalakshmi, K., Pramod Kumar, M., Madakka, M., & Vijayanand, P. (2022). Evaluation of heavy metal pollution from coastal water of Nizampatnam Bay and Lankevanidibba, East Coast of India. *Journal of Sea Research*, *186*(May), 102232. https://doi.org/10.1016/j.seares.2022.102232
14. Lo, L.S.H., Liu, X., Liu, H., Shao, M., Qian, P.-Y., & Cheng, J. (2023). Aquaculture bacterial pathogen database: Pathogen monitoring and screening in coastal waters using environmental DNA. *Water Research X*, *20*, 100194. https://doi.org/https://doi.org/10.1016/j.wroa.2023.100194
15. Lucia, G., Giuliani, M.E., d'Errico, G., Booms, E., Benedetti, M., Di Carlo, M., Fattorini, D., Gorbi, S., & Regoli, F. (2023). Toxicological effects of cigarette butts for marine organisms. *Environment International*, *171*, 107733. https://doi.org/https://doi.org/10.1016/j.envint.2023.107733
16. Mu, X., Yuan, L., Meng, S., Huang, Y., Chen, J., & Li, Y. (2023). Significant decline of water pollution associated with inland fishery across China. *Eco-Environment & Health*, *2*(2), 79–87. https://doi.org/https://doi.org/10.1016/j.eehl.2023.05.002
17. Muis, R., Al Fariz, R.D., Yunus, S., Tasrief, R., Rachman, I., & Matsumoto, T. (2024). Investigating the potential of landfilled plastic waste – A case study of makassar landfill, Eastern Indonesia. *Ecological Engineering and Environmental Technology*, *25*(3), 185–196. https://doi.org/10.12912/27197050/178529
18. Rajendiran, D., Harikrishnan, N., & Veeramuthu, K. (2025). Heavy metal concentrations and pollution indicators in the Ennore ecosystem, east coast of Tamilnadu, India using atomic absorption spectrometry study with statistical approach. *Scientific Reports*, *15*(1). https://doi.org/10.1038/s41598-025-93484-6
19. Tansel, B. (2024). Geographical characteristics that promote persistence and accumulation of PFAS in coastal waters and open seas: Current and emerging hot spots. *Environmental Challenges*, *14*, 100861. https://doi.org/https://doi.org/10.1016/j.envc.2024.100861
20. Thelen, T., Anarde, K., Dietrich, J.C., & Hino, M. (2024). Wind and rain compound with tides to cause frequent and unexpected coastal floods. *Water Research*, *266*, 122339. https://doi.org/https://doi.org/10.1016/j.watres.2024.122339
21. Uddin, M.G., Rahman, A., Rosa Taghikhah, F., & Olbert, A.I. (2024). Data-driven evolution of water quality models: An in-depth investigation of innovative outlier detection approaches - A case study of Irish Water Quality Index (IEWQI) model. *Water Research*, *255*, 121499. https://doi.org/https://doi.org/10.1016/j.watres.2024.121499
22. Wu, J., Rong, S., Wang, M., Lu, R., & Liu, J. (2022). Environmental quality and ecological risk assessment of heavy metals in the Zhuhai Coast, China. *Frontiers in Marine Science*, *9*. https://doi.org/10.3389/fmars.2022.898423
23. Xianglei, L., Xiaohong, S., Guangchao, L., Zongwen, Z., Xiaonan, W., Qingjia, M., Ruizhi, L., & Wenwen, L. (2025). The derivation of seawater quality criteria and ecological risk assessment of Tonalide. *Ecotoxicology and Environmental Safety*, *298*, 118287. https://doi.org/https://doi.org/10.1016/j.ecoenv.2025.118287
24. Zou, Y., Lou, S., Zhang, Z., Liu, S., Zhou, X., Zhou, F., Radnaeva, L.D., Nikitina, E., & Fedorova, I.V. (2024). Predictions of heavy metal concentrations by physiochemical water quality parameters in coastal areas of Yangtze river estuary. *Marine Pollution Bulletin*, *199*, 115951. https://doi.org/https://doi.org/10.1016/j.marpolbul.2023.115951